UNCLASSIFIED

SECURITY CLASSIFICATION OF THIS PAGE

REPORT DOCUMENTATION PAGE

1a. REPORT SECURITY CLASSIFICATION Unclassified	1b. RESTRICTIVE MARKINGS None
2a. SECURITY CLASSIFICATION AUTHORITY	3. DISTRIBUTION/AVAILABILITY OF REPORT Approved for public release; distribution is unlimited.
2b. DECLASSIFICATION/DOWNGRADING SCHEDULE	
4. PERFORMING ORGANIZATION REPORT NUMBER(S) NORDA Report 220	5. MONITORING ORGANIZATION REPORT NUMBER(S) NORDA Report 220
6. NAME OF PERFORMING ORGANIZATION Naval Ocean Research and Development Activity	7a. NAME OF MONITORING ORGANIZATION Naval Ocean Research and Development Activity
6c. ADDRESS *(City, State, and ZIP Code)* Ocean Acoustics and Technology Directorate NSTL, Mississippi 39529–5004	7b. ADDRESS *(City, State, and ZIP Code)* Ocean Acoustics and Technology Directorate NSTL, Mississippi 39529–5004
8a. NAME OF FUNDING/SPONSORING ORGANIZATION Naval Ocean Research and Development Activity 8b. OFFICE SYMBOL *(If applicable)*	9. PROCUREMENT INSTRUMENT IDENTIFICATION NUMBER
8c. ADDRESS *(City, State, and ZIP Code)* Ocean Acoustics and Technology Directorate NSTL, Mississippi 39529–5004	10. SOURCE OF FUNDING NOS. PROGRAM ELEMENT NO. 61153N; PROJECT NO. 03105; TASK NO. 330; WORK UNIT NO. 12458C
11. TITLE *(Include Security Classification)* Low Frequency Seismo-Acoustic Propagation in a Sloping Ocean Environment: Measured Results and Numerical Predictions	
12. PERSONAL AUTHOR(S) Hassan B. Ali, L. Dale Bibee, Mona Authement*; Ralph A. Stephen**; Jeff Becklehimer***	
13a. TYPE OF REPORT Final	13b. TIME COVERED From _____ To _____
14. DATE OF REPORT *(Yr., Mo., Day)* November 1987	15. PAGE COUNT 14
16. SUPPLEMENTARY NOTATION *NORDA, **Woods Hole Oceanographic Institution, and ***ODSI Defense Systems, Inc.	
17. COSATI CODES FIELD / GROUP / SUB. GR.	18. SUBJECT TERMS *(Continue on reverse if necessary and identify by block number)* ocean water column, sea bottom, sound propagation, seismic wave, waterborne sound source, frequency

19. ABSTRACT *(Continue on reverse if necessary and identify by block number)*

As part of the continuing program to investigate the characteristics of acoustic propagation and ambient noise in the very low frequency regime (20 Hz and less), the Naval Ocean Research and Development Activity (NORDA) conducted ninety-seven experiments off the Southeastern coast of the U.S. (Cape Fear) in 1985.

Preliminary results of the Cape Fear data analysis have already shed some light on seismo-acoustic propagation. At the source-receiver ranges thus far considered, considerable penetration into the bottom is evident, particularly at frequencies below about 20 Hz. Both body and Scholte waves appear to contribute to the propagation in the sediment. Under certain conditions, the net S/N ratio of the vertical geophone sensor is at least 6 dB higher than that of the hydrophone.

Although examination of the depth dependence of the waterborne transmission loss as a function of range is still in process, spot checks at several ranges do indicate agreement between the model (IFDPE) and measured results (hydrophone array). The SAFARI and IFDPE models provide some insight into certain aspects of the propagation, but alone, neither is sufficient for the environment considered. It is expected that models based on the finite difference method will be more appropriate.

20. DISTRIBUTION/AVAILABILITY OF ABSTRACT UNCLASSIFIED/UNLIMITED ☐ SAME AS RPT. ■ DTIC USERS ☐	21. ABSTRACT SECURITY CLASSIFICATION Unclassified
22a. NAME OF RESPONSIBLE INDIVIDUAL Hassan B. Ali	22b. TELEPHONE NUMBER *(Include Area Code)* (601) 688-5736
	22c. OFFICE SYMBOL Code 245

DD FORM 1473, 83 APR EDITION OF 1 JAN 73 IS OBSOLETE

UNCLASSIFIED

SECURITY CLASSIFICATION OF THIS PAGE

Naval Ocean Research and Development Activity
November 1987
Report 220

Low Frequency Seismo-Acoustic Propagation in a Sloping Ocean Environment: Measured Results and Numerical Predictions

Published in *Acoustics and the Ocean Bottom*, the proceedings of the II Federation of Acoustical Societies of Europe Conference (F.A.S.E.), Madrid, June 1987. Consejo Superior de Investigaciones Cientifices (C.S.I.C.), Madrid.

Hassan B. Ali
L. Dale Bibee
Mona J. Authement
Ocean Acoustics Division
Ocean Acoustics and Technology Directorate

Ralph A. Stephen
Woods Hole Oceanographic Institution
Woods Hole, Massachusetts

Jeff Becklehimer
ODSI Defense Systems, Inc.
6110 Executive Boulevard
Rockville, Maryland

Foreword

An understanding of the characteristics of very low frequency (VLF) sound propagation in the ocean is essential for the effective use of naval systems. One aspect—namely, the interaction of waterborne energy with the ocean bottom—is particularly important in bottom-limited environments, especially at VLF frequencies.

This report presents the preliminary findings of measurements conducted by NORDA in an area off Cape Fear, North Carolina. The results offer insight into the phenomena associated with energy partitioning between waterborne and bottom paths, and provide some information on the utility of standard numerical propagation models.

William B Moseley

W. B. Moseley
Technical Director

A C Esau

A. C. Esau, Captain, USN
Commanding Officer

Executive summary

Generally speaking, the ocean water column offers a far more favorable medium for the propagation of sound than does the sea bottom. In certain circumstances, however, the energy emitted from a waterborne sound source may travel more readily in the sea floor, as a seismic wave, than in the water column itself. This is particularly true for low frequency propagation in those cases in which substantial interaction with the bottom occurs. The successful exploitation of such propagation, for example for the seismic sensing of very low frequency waterborne signals, requires an understanding of both the responsible mechanisms and their range of applicability.

As part of the continuing program to investigate the characteristics of acoustic propagation and ambient noise in the very low frequency regime (20 Hz and less), the Naval Ocean Research and Development Activity (NORDA) conducted an experiment off the Southeastern coast of the U.S. (Cape Fear) in 1985.

Preliminary results of the Cape Fear data analysis have already shed some light on seismo-acoustic propagation. At the source-receiver ranges thus far considered, considerable penetration into the bottom is evident, particularly at frequencies below about 20 Hz. Both body and Scholte waves appear to contribute to the propagation in the sediment. Under certain conditions, the net S/N ratio of the vertical geophone sensor is at least 6 dB higher than that of the hydrophone.

Although examination of the depth dependence of the waterborne transmission loss as a function of range is still in process, spot checks at several ranges do indicate agreement between the model (IFDPE) and measured results (hydrophone array). The SAFARI and IFDPE models provide some insight into certain aspects of the propagation, but alone, neither is sufficient for the environment considered. It is expected that models based on the finite difference method will be more appropriate.

Acknowledgments

The work reported here was accomplished as part of NORDA's 6.1 efforts (Program Element 61153N) for the Office of Naval Research (ONR). The authors would particularly like to express their appreciation for the encouragement received from the Head of ONR.

Contents

Low Frequency Seismo-Acoustic Propagation in a Sloping Ocean Environment: Measured Results and Numerical Predictions

Introduction

For a variety of reasons, there is considerable interest in the propagation of low-frequency sound in bottom-limited environments, including shallow-water and sloping ocean bottoms. In such environments the generally favorable water column conditions characterizing "deep - water" propagation are often absent. Instead, significant interaction with the ocean bottom can severely degrade a waterborne signal and, in some cases, lead to the result that the bottom path becomes a significant means of propagation. Ducted (wave-guide) propagation in shallow water is a familiar example of the preceding. In this case the degree of bottom interaction (and, hence, energy loss) depends on the ratio of acoustic wavelength (λ) to water depth (H), among other things. The bottom loss increases with increasing λ/H until, eventually, a frequency is reached below which effective propagation in the water column ceases to exist. Nevertheless, even below this "cut-off frequency" for waterborne signals, the bottom can be an important path for interface and other seismic waves.[1,2]

Propagation along bottom slopes, particularly in the direction of decreasing water depth ("upslope"), is another situation in which significant bottom penetration can take place. The increasing grazing angle of the sound "ray," with increasing distances up the slope, eventually results in sizable penetration into the slope at the critical angle of the bottom. In other words, at the critical angle acoustic energy is converted from the discrete, trapped spectrum into the continuous spectrum. The point in range at which this conversion occurs for the ray corresponds to the cutoff depth of the equivalent mode.[3] For isovelocity conditions in the sediment (the usual assumption of much of the earlier modeling efforts) the continuous spectrum is largely "lost" into the deeper, basement levels of the subbottom. However, as shown by Miller et al. (this volume), for the more realistic case of a positive sound-speed gradient in the sediment, the sound refracted into the bottom beyond its mode cutoff may continue traveling upslope in the sediment beyond the cutoff range, and reach a point closer to shore. Other data from Del Balzo, et al., suggest that under certain conditions the propagation of signal and noise may be characterized by differential "stripping" in sloping environments, leading to significant signal-to-noise (S/N) gains along portions of the slope.

Numerous other examples can be cited. However, efforts to understand very low frequency (VLF) propagation in bottom-limited environments clearly must address both waterborne and bottom paths, particularly the energy partitioning among the paths.

As part of its ongoing efforts to understand the preceding aspects of seismo-acoustic propagation in the VLF domain, the Naval Ocean Research and Development Activity (NORDA) is conducting experiments in relevant ocean environments. This paper will present preliminary results of the measurements in one area and discuss predictions based on well-known numerical models.

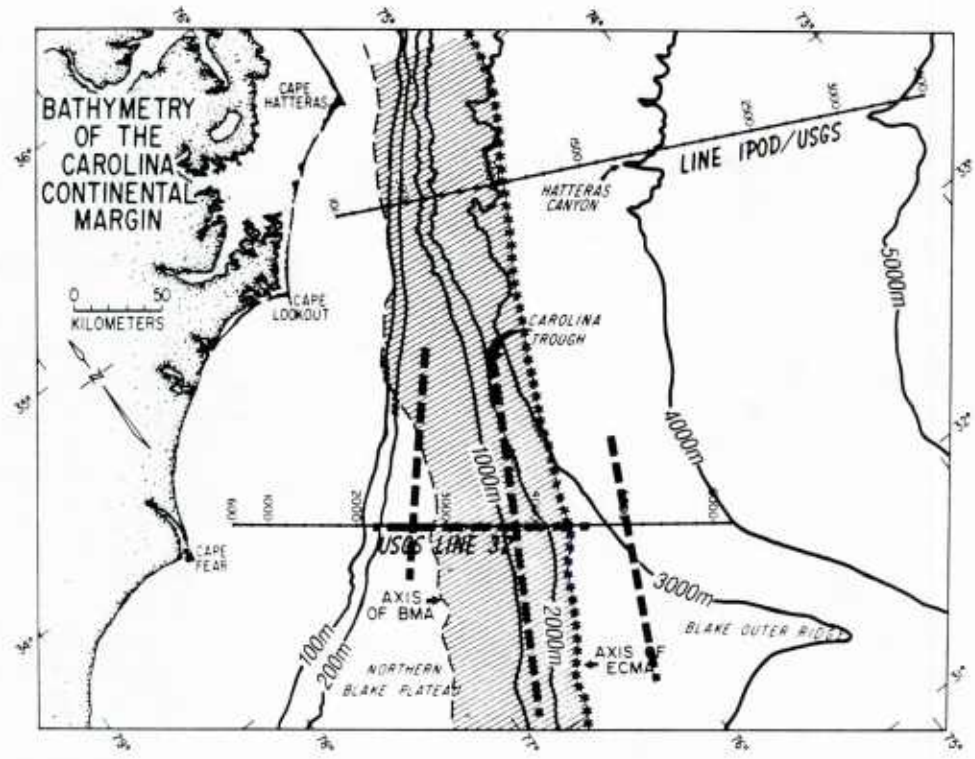

Figure 1. Cape Fear bathymetry and test geometry.

The Experiment

The NORDA experiment was conducted in collaboration with the U.S. Geological Survey (USGS) and Scripps Institution of Oceanography. The experiment area was located along the continental slope of the southeastern U.S., off Cape Fear, North Carolina. Figure 1 provides some details of the test area and the geometry of the runs.

For the geometry shown, an extensive series of runs was made using a continuous wave (CW) source (10 Hz), air-guns (1000 in^3), and explosives (45 kg TNT). The resulting signals were received by a 300-m long vertical array of 16 hydrophones (20-m spacing) placed at the shallow end of the slope and 15 ocean bottom seismometers (OBS) distributed on the slope. The hydrophone signals were multiplexed and telemetered via UHF to a nearby ship, where they were converted at a 1300-Hz sampling rate. The OBS signals, on the other hand, were recorded and stored by the OBS electronics for subsequent playback and analysis.

Selected Results of the Measurements

Analysis of the OBS data set has shown that for all source-receiver separations significant amounts of acoustic energy are partitioned into paths traveling through the sea floor at VLF frequencies. Figure 2 shows power spectra from signals traveling along specific paths from an explosive source to a vertical geophone receiver resting

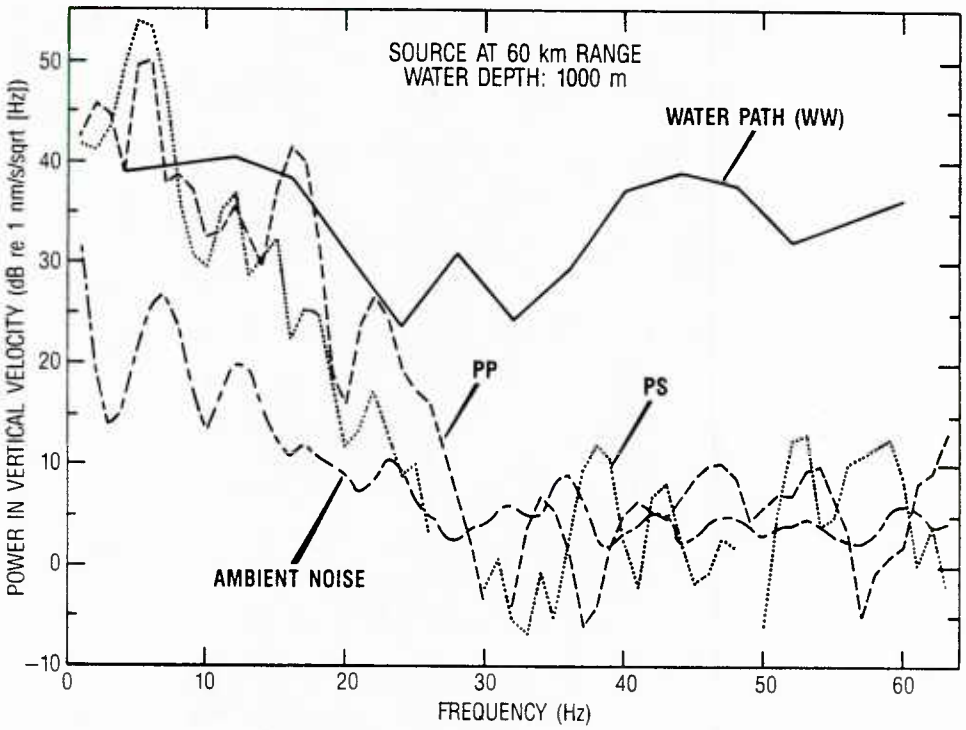

Figure 2. Spectral content of various travel paths recorded on a vertical geophone.

on the sea floor 60 km away. The water path has traveled primarily through the water column, interacting with the bottom at most by reflecting from it. PP is a compressional wave which is refracted through the sedimentary section and returns to the surface. PS travels as a compressional wave through most of the travel path, but converts to a shear wave beneath the receiver and traverses the uppermost sedimentary section in a shear mode. Ambient noise just before the shot was detonated is shown for reference. At frequencies higher than 25 Hz, the water path signal contains much more energy than those paths traveling through the seafloor. However, at frequencies below 25 Hz both the compressional and shear wave energy are comparable to the water path signals. It is reasonable to expect that significant energy is being partitioned into a bottom at all frequencies, but that frequency-dependent propagation through the sea floor is responsible for the observed differences in water path and sea floor path spectra.

The importance of sea floor transmission paths can also be seen in the time domain. Figure 3 shows the signal from an air gun source 8 km away from a vertical geophone sensor. The unfiltered data is shown along with the signal bandpass filtered into two different bands. The sediment refraction (ground path) and water path are readily distinguishable on the basis of frequency content. In the 2-10 Hz band the ground path and water path signals are of roughly equal amplitude. However, from 20-40 Hz the water path is clearly dominant because the ground path was significantly attenuated.

In addition to body wave transmission through the sea floor, the difference in characteristics of the geophone and OBS hydrophone signals indicates significant

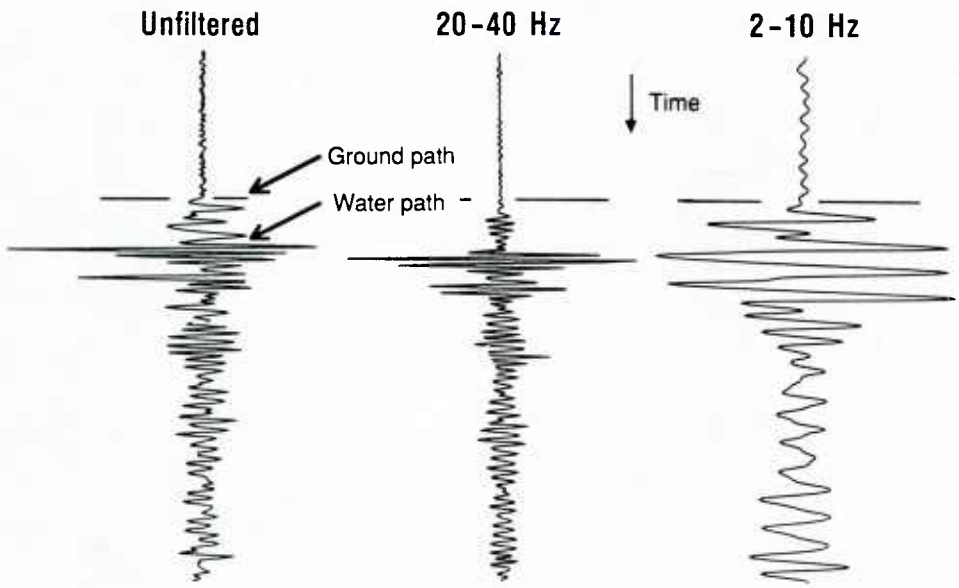

Figure 3. Vertical geophone response to an 8-km distant airgun shot.

excitation of secondary Scholte waves at the water-sediment interface, probably due to scattering from nearby bottom features. This generates a 6-dB increase in S/N ratio for a geophone sensor as opposed to a hydrophone sensor in the VLF band (Figure 4). The S/N ratio for a 45 kg explosive shot at 65 km range is computed by calculating the spectrum of a window of data, including the entire signal coda and dividing by the spectrum of an ambient noise sample of equal length taken just prior to the shot. The vertical geophone shows a consistent 6 dB advantage in S/N ratio when compared to a hydrophone less than 1 m away.

The Numerical Models

General Overview

Several models were used for the Cape Fear calculations, including IFDPE, PAREQ, SNAP, and SAFARI. Of these models, results from only IFDPE and SAFARI will be discussed here. In addition, "generic" results from a finite difference model will be shown.

The IFDPE (Implicit Finite Difference Parabolic Equation) is a wide-angle ($\pm 40^{\circ}$) model based on the parabolic equation. Its ability to handle a range-dependent environment was the main reason for its choice. However, the IFDPE cannot handle shear effects in the bottom. For the latter effects, which are important for the Cape Fear experiment, the SAFARI model was used. SAFARI, the SACLANT Centre's Fast Field Program, is a full-wave model capable of handling both discrete and continuous propagation in the water column and elastic bottom. However it is restricted to propagation in horizontally stratified media and cannot, therefore, handle range-dependent propagation.

Environmental Input

The geoacoustic input parameters for SAFARI are shown in Figure 5. Although based on the actual Cape Fear environment (CTD casts and seismic-derived forma-

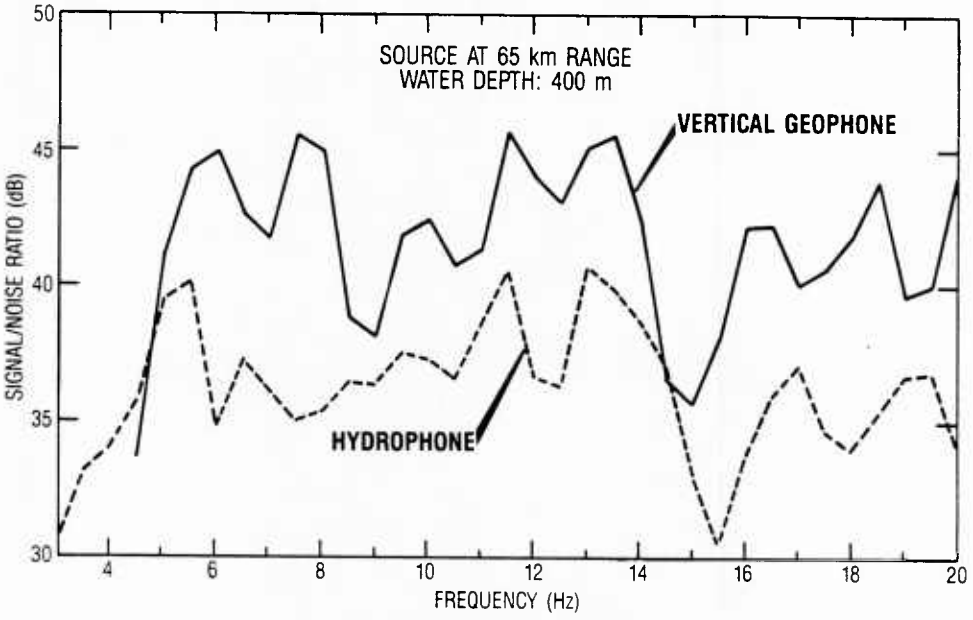

Figure 4. Relative S/N ratio for geophone and hydrophone sensors.

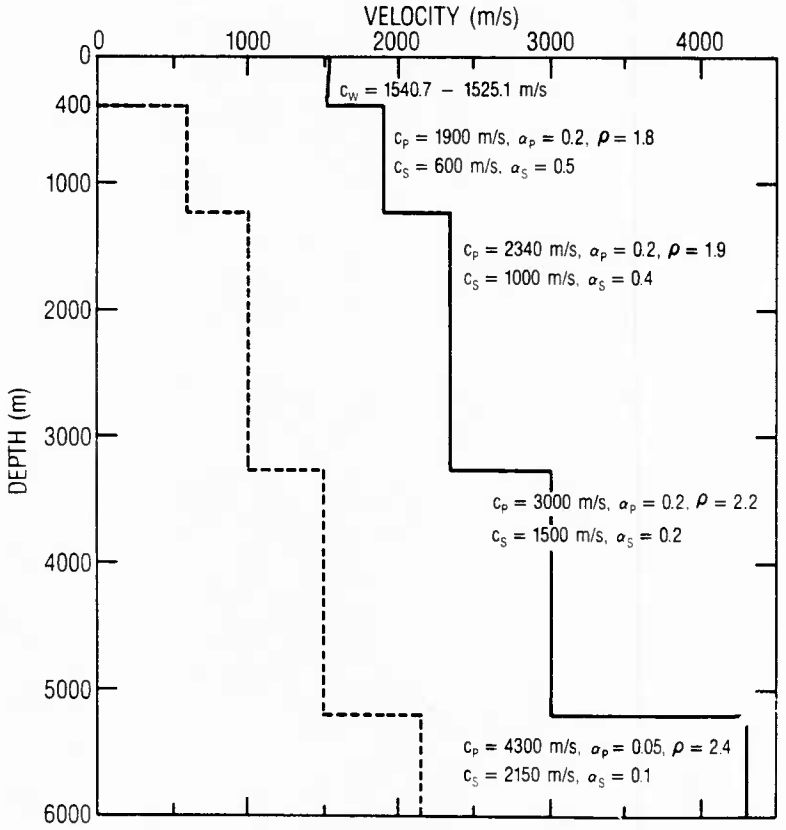

Figure 5. Geoacoustic input parameters for SAFARI model.

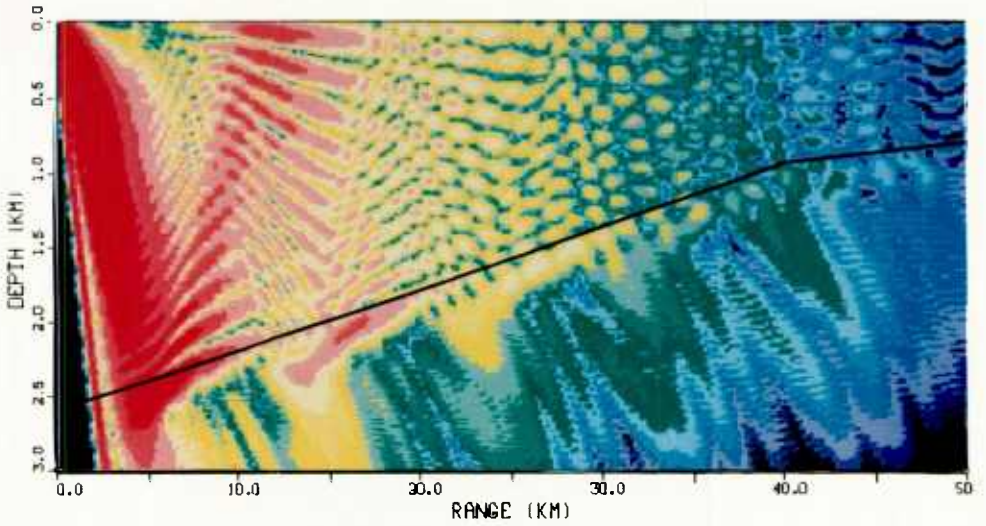

Figure 6. Predicted (IFDPE) upslope propagation for Cape Fear.

tion velocities), the parameters are nevertheless a simplification. In particular: gradients in the bottom are not accounted for, the shear values are estimates and, most important, the water depth is assumed to be a constant 400 m (the water depth at the location of the hydrophone array).

For the IFDPE, the same sound speed profile was used for the water column; for the bottom an isovelocity bottom with compressional speed of 1900 m/s was used, although multilayered bottoms are possible with this model. The preceding profile is strictly valid at only one field point. The profile was extended throughout the field, and was, of course, subject to the constraints of the slope geometry. The range-dependence was thereby restricted solely to the bathymetry. The bottom varied in depth from 2600 m to 250 m over a range of 100 km.

Selected Numerical Results

Because of space limitations, the discussions will be confined to upslope propagation, Figure 6 being a typical IFDPE result for a 10 Hz source at a depth of 100 m. Penetration into the bottom occurs both close to the source and as energy proceeds up the slope, at several depths corresponding to the respective modal cutoff points. The transmission loss at a particular receiver depth (100 m) is compared with that from SAFARI in Figure 7. At very short ranges (<10 km) the IFDPE results are inaccurate, since very high angle propagation is not modeled. At intermediate ranges, there is fair agreement between the two models. However, with increasing propagation up the slope, the results differ. In particular, SAFARI underestimates (by as much as 20 dB) the longer range losses. This is quite plausible, since the flat bottom assumed by SAFARI does not account for the considerable energy transfer from waterborne to bottom paths caused by the slope.

It is noted that the Green's function (FFP integrand) obtained from SAFARI for this case is consistent with the modal behavior suggested by Figure 6. In particular, three discrete waterborne modes dominate the propagation, with much smaller amplitude trapped and continuous modes evident between the various bottom layers. The result of

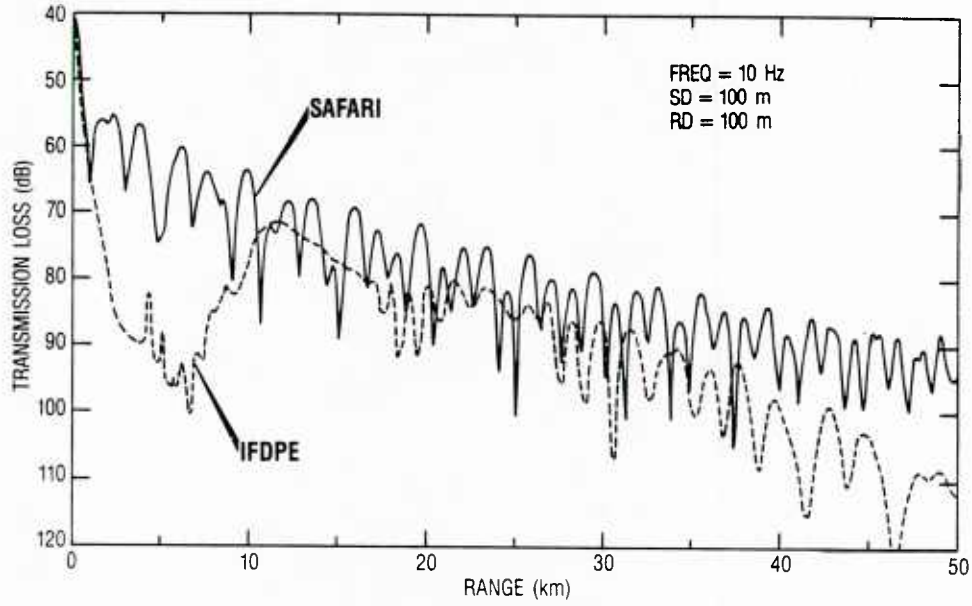

Figure 7. Comparison of SAFARI and IFDPE transmission losses at 100 m depth.

a pulse calculation using SAFARI is shown in Figure 8. The pulse, with a peak amplitude at 10 Hz and a depth of 85 m, was designed to simulate the response of the explosives used in the experiment. The response with range is plotted against time reduced by 4.3 km/s, the speed of the deepest layer in the model (Figure 5). The waterborne arrivals are clearly dominant, separating with range into 3 or 4 discrete modes. Preceding the water arrivals, the head waves along the various bottom layers are evident, albeit with reduced amplitudes. For source and receivers closer to the bottom than shown here, the model predicts another dominant mode, a Scholte interface wave propagating with a velocity of approximately 523 m/s.

Finite Difference Model

We now show how the finite difference method can be used to solve range-dependent geoacoustic propagation problems[5,6,7] using propagation in a continental margin model as a generic example. Figure 9 shows the time series record sections at two gains for a laterally homogeneous channel. Figure 10 shows the velocity-depth functions for P and S waves and the density-depth function. The water layer is 97.5 m thick and the velocity profile in the channel is uniform. The seabed corresponds to soft sediments and a gradient in elastic parameters and density is present in the upper 250 m. The source waveform in pressure is the third derivative of a Gaussian curve with a peak frequency of 10 Hz and an upper half-power frequency of 13.5 Hz.[5] By considering the time evolution of a band-limited source, we obtain both the amplitude and phase of the propagation response. The source is located at 40 m depth, just above the center of the waveguide, and the receivers are at 45 m depth. The finite difference solution is carried out in the time-space domain, so we simply start up the disturbance at the source location and watch the outgoing wavefield as it propagates down the waveguide.

Figure 9 shows the time series response at a number of receivers from 0.0 to 4.0 km range at a depth of 45 m. Since the model is essentially a layer over an elastic half-

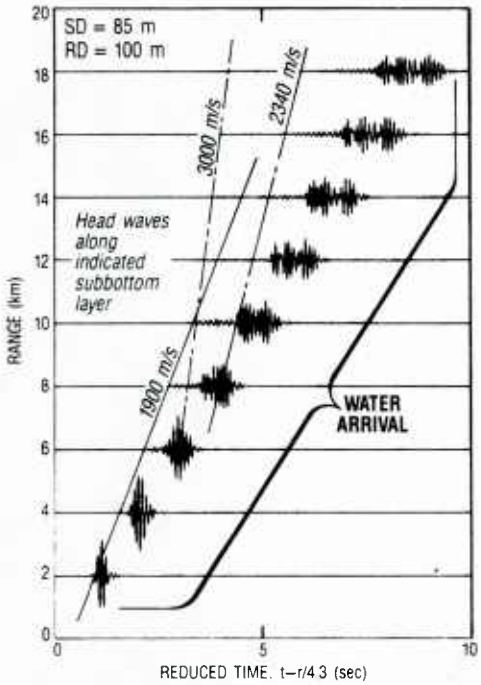

Figure 8. Result of a SAFARI pulse calculation for a simplified Cape Fear environment.

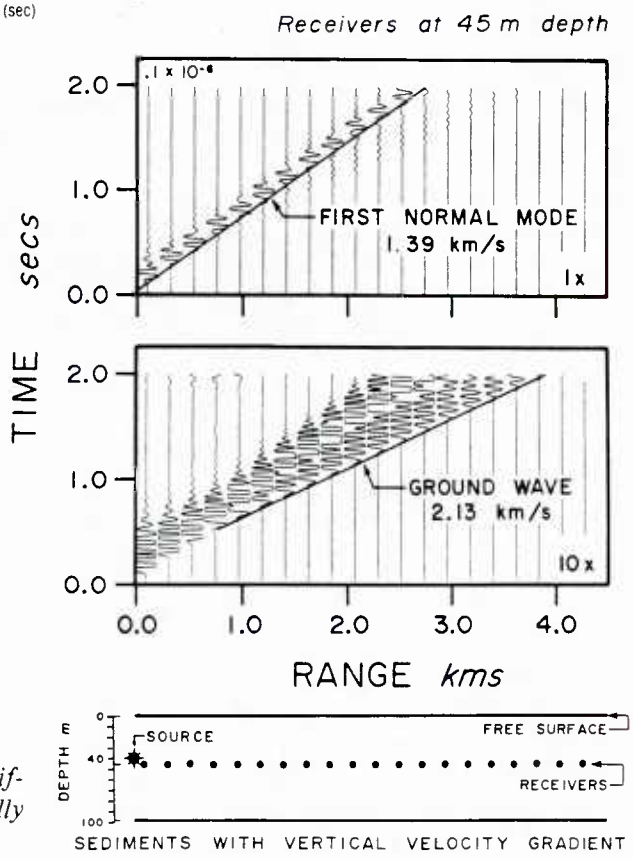

Figure 9. Example of finite difference results for a laterally homogeneous channel.

space, we get the two principal arrivals predicted by Pekeris.[9] The first arrival is the wave, traveling in this case at 2.13 km/s, which corresponds to the compressional wave velocity of the bottom. When this energy, which has dived into the bottom, returns to the water column, it reverberates like the normal modes and creates a "ringing" packet. At every interaction with the bottom this packet leaks energy into shear waves and compressional waves. If the shear wave velocity were zero we would identify this packet as a compressional leaky mode.

The second arrival is predominantly waterborne energy, corresponding to the first normal mode. The cutoff frequencies for the first and second modes in this model are 5.8 Hz and 17.4 Hz, so at 10 Hz only the first mode is supported. This energy is super-critical for compressional waves and would be totally trapped if the shear velocity were zero. However, because the shear velocity is less than the water velocity, this packet also continually leaks shear energy into the bottom. It has a group velocity of 1.39 km/s, slightly less than the compressional wave velocity in water. After the normal mode an exponentially decaying packet corresponds to the Airy phase.

For receivers closer to the sea floor this model contains a third dominant arrival, the Stoneley wave. This wave is evanescent both upward and downward from the boundary and propagates with a velocity of 0.60 km/s, slightly less than the shear speed in the sediments. It is not observed in Figure 9 because the receivers are too far off the bottom.

We next consider a range-dependent model (Figure 11). The model is the same as Figure 9 out to 1.25 km from the source, at which point the bottom drops away at an angle of 11.3°. This represents approximately the steepest slope observed on continental margins. The velocity-depth and density-depth functions below the sea floor are the same as in Figure 10. There are three significant observations here. First, the first normal mode decays with range beyond the shelf break. Its group velocity increases to 1.5 km/s and it becomes a direct water wave.

The second observation is a weak lateral reflection of the first normal mode back from the top of the wedge. The third observation is that the ground wave arrives later at receivers above the wedge. This is expected because the ground energy is traveling up through a progressively thicker, slow-velocity water column. The apparent velocity of these arrivals is 1.89 km/s. The amplitudes of the ground wave above the wedge are slightly larger at the same range than in the absence of the wedge because of focusing around the shelf break.

The above examples demonstrate the applicability of the finite difference method to geoacoustic propagation in range-dependent waveguides.

Conclusions

Attempts to understand VLF propagation must, perforce, consider both the waterborne and bottom paths. particularly the partitioning of energy between them. Preliminary results of the Cape Fear data analysis have already shed some light on the preceding. At the source-receiver ranges thus far considered, considerable penetration into the bottom is evident, particularly at frequencies below about 20 Hz. Both body and Scholte waves appear to contribute to the propagation in the sediment. Under certain conditions, the net S/N ratio of the vertical geophone sensor is at least 6 dB higher than that of the hydrophone.

Although examination of the depth dependence of the waterborne transmission loss as a function of range is still in process, spot checks at several ranges do indicate

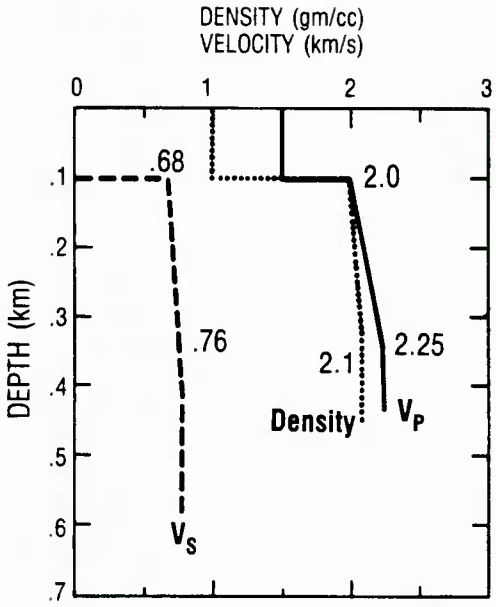

Figure 10. Velocity depth functions for P and S waves and density–depth function.

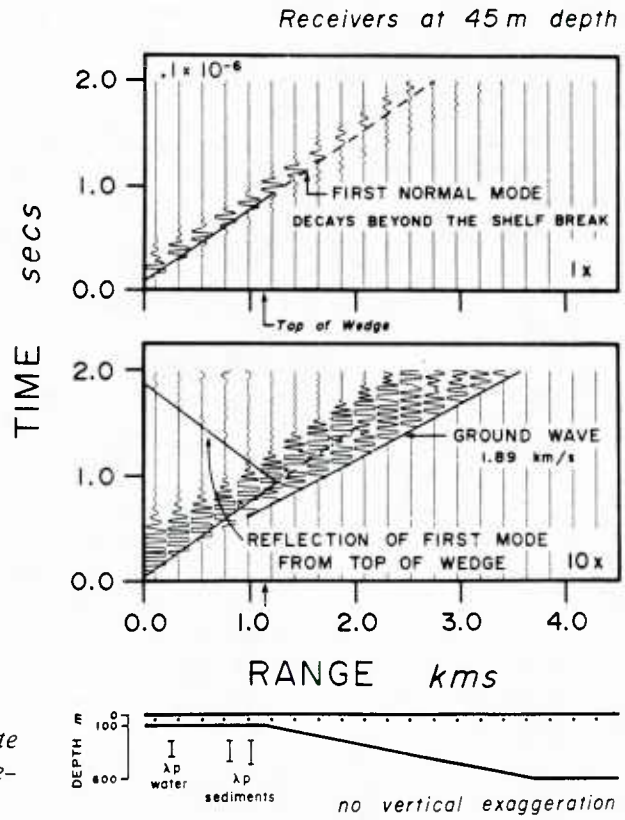

Figure 11. Example of finite difference results for a range-dependent channel.

agreement between the model (IFDPE) and measured results (hydrophone array). The SAFARI and IFDPE models provide some insight into certain aspects of the propagation, but alone, neither is sufficient for the environment considered. It is expected that models based on the finite difference method will be more appropriate.

References

1. Rauch, D. and Schmalfeldt, B., *Explosion-generated Seismic Interface Waves in Shallow Water: Experimental results.* SACLANTCEN SR-71, La Spezia, Italy (1983).

2. Ali, H. B. and Schmalfeldt, B., *Seismic Sensing of Low-Frequency Radiated Ship Noise*, SACLANTCEN SR-77, La Spezia, Italy (1984).

3. Jensen, F. B. and Kuperman, W. A., 1980, Sound Propagation in a Wedge-Shaped Ocean with Penetrable Bottom, *J. Acoust. Soc. Am.* 67: 1564-1566 (1980).

4. Del Balzo, D. R., J. E. Matthews, J. V. Soileau, and C. Feuillade, "Acoustic Propagation Over Large-Scale Linear Ocean Slopes," In: Akal, T. and Berkson, J. (eds.), In *Proceedings, Ocean Seismo-Acoustics*, New York, Plenum Press (1986).

5. Stephen, R. A., A Comparison of Finite Difference and Reflectivity Seismograms for Marine Models, *Geophys. J. R. Astr. Soc.* 72: 39-58 (1983).

6. Bhasavanija, K., *A Finite Difference Model of an Acoustic Logging Tool: the Borehole in a Horizontally Layered Geologic Medium*, Ph.D. Thesis, Colorado School of Mines, Golden, Colorado (1983).

7. Nicoletis, L., *Simulation numerique de la propagation d'ondes sismiques dans less milieux stratifies a deux et trois dimensions; contribution a la construction et a l'interpretation des sismogrammes synthetiques*, Ph.D. Thesis, L'universite Pierre et Marie Curie, Paris VI (1981).

8. Stephen, R. A., F. Pardo-Casas, and C. H. Cheng, Finite-Difference Synthetic Acoustic Logs, *Geophysics* 50: 1588-1609 (1985).

9. Pekeris, C. L., Theory of Propagation of Explosive Sound in Shallow Water, *Geological Society of America*, Memoir 27 (1948).

Current Standard Distribution List

ASN (RE&S)
CNO (OP-951)
CNO (OP-987)
NODC (G. W. Withee)
CNO (OP-096)
NAVAIRDEVCEN
NAVAIRSYSCOMHDQR
NAVCOASTSYSCEN
SPANAVWARSYSCOM
NAVENVPREDRSHFAC
NAVFACENGCOMHDQRS
NORDA (Code 105)
NORDA (Code 115)
NORDA (Code 200)
NORDA (Code 300)
NRL
CNOC
FLENUMOCEANCEN
NAVOCEANO
NAVOCEANSYSCOM
ONRBRO LONDON
ONRWEST
DTSRDC
NSWC
NUSC
NAVPGSCOL
ONL
NUSCDET (New London)
DTIC (12)
ONR
WHOI
SCRIPPS
NAVSURWPNCEN
DMA
INO
ARL/Texas
APL/University of Washington
DARPA
NPOC
NWOC
NEOC

Distribution List (Continued)

Gerald A. Cann, Inc..
1710 Goodridge Drive
McLean, VA 22102

Mr. John Schuster
1931 Jefferson Davis Highway
Arlington, VA 22202

Mr. Charles Stuart
Defense Advanced Research Projects Agency
1400 Wilson Boulevard
Arlington, VA 22209

Dr. J. B. Orcutt
Institute of Marine Resources
Scripps Institution of Geophysics
& Planetary Physics
University of California
La Jolla, CA 92093

Dr. Randall S. Jacobson
Code 1125GG
Office of Naval Research
800 N. Quincy St.
Arlington, VA 22217-5000

Mr. Charles Votaw
Office of Naval Technology
800 N. Quincy St.
Arlington, VA 22217-5000

Dr. William Farrell
Science Applications International Corp.
10210 Campus Point Drive
San Diego, CA 92121

Dr. Charles Spofford
Science Applications International Corp.
10210 Campus Point Drive
San Diego, CA 92121

Mr. W. F. Monet
Science Applications International Corp.
10210 Campus Point Drive
San Diego, CA 92121

Mr. James Dafoe
Systems Planning & Analysis, Inc.
5111 Leesburg Pike
Falls Church, VA 22041

Mr. R. A. Stephen
Woods Hole Oceanographic Institute
86-96 Water St.
Woods Hole, MA 02543

L. Parish (PMW 180-4)
Space & Naval Warfare Systems Command
Washington, DC 20363-5100

K. Hawker (PMW-180-4)
Space & Naval Warfare Systems Command
Washington, DC 20363-5100

LT F. Ogg (PMW-180-4)
Space & Naval Warfare Systems Command
Washington, DC 20363-5100

R. Mitnick (PMW 180-4)
Space & Naval Warfare Systems Command
Washington, DC 20363-5100

CAPT K. Evans (PMW 180-4)
Space & Naval Warfare Systems Command
Washington, DC 20363-5100

Commanding Officer
NORDA
Attn: B. Adams (Code 113)
NSTL, MS 39529-5004

Commanding Officer
NORDA
Attn: D. Del Balzo (Code 244)
NSTL, MS 39529-5004

Commanding Officer
NORDA
Attn: J. Matthews (Code 220)
NSTL, MS 39529-5004

Commanding Officer
NORDA
Attn: R. Wagstaff (Code 245)
NSTL, MS 39529-5004

ONR Det
Attn: E. D. Chaika
NSTL, MS 39529-5004

Chief of Naval Research
800 North Quincy St
Arlington, VA 22217-5000

R. F. Obrochta (Code 425AR)
Office of Naval Research
800 North Quincy St.
Arlington, VA 22217-5000

R. Fitzgerald (Code 425UR)
Office of Naval Research
800 North Quincy St.
Arlington, VA 22217-5000

Distribution List (Concluded)

J. Heacock (Code 425GG)
Office of Naval Research
800 North Quincy St.
Arlington, VA 22217-5000

F. E. Saalfield (Code 400)
Office of Naval Research
800 North Quincy St.
Arlington, VA 22217-5000

E. J. Wegman (Code 411)
Office of Naval Research
800 North Quincy St.
Arlington, VA 22217-5000

G. Hamilton (Code 420)
Office of Naval Research
800 North Quincy St.
Arlington, VA 22217-5000

D. L. Bradley (Code 425)
Office of Naval Research
800 North Quincy St.
Arlington, VA 22217-5000

A. Diness (Code 430)
Office of Naval Research
800 North Quincy St.
Arlington, VA 22217-5000

M. McKisic (Code 325A)
Office of Naval Research
800 North Quincy St.
Arlington, VA 22217-5000

T. Warfield (220B)
Office of Naval Research
800 North Quincy St.
Arlington, VA 22217-5000

O. Diachok (Code 5128)
Naval Research Laboratory
Washington, DC 20375

R. Dicus (Code 5128)
Naval Research Laboratory
Washington, DC 20375

L. Sternberg
Office of Naval Research
495 Summer St.
Boston, MA 02210

H. P. Bucker
Naval Ocean Systems Center
San Diego, CA 92152-5000

R. Bachman (Code 541)
Naval Ocean Systems Center
San Diego, CA 92152-5000

E. L. Hamilton (Code 541)
Naval Ocean Systems Center
San Diego, CA 92152-5000

M. A. Pederson
Naval Ocean Systems Center
San Diego, CA 92152-5000

Chief of Naval Operations
Attn: (OP 006) CDR C. Spikes
Washington, DC 20350

Chief of Naval Operations
Attn: (OP 952D) CDR L. Dantzler
Washington, DC 20350